Quality Assurance of Radiotherapy Treatment Using Scattered X-ray

Students: Tatiana Kashtanova, Samuel Ydenberg

Mentors: Dr. Xun Jia, Dr. Lin Su, Dr. Yujie Chi, Dr. Youfang Lai, Dr. Xiaoyu Hu

Abstract

In this project, we implemented a quality assurance method for radiation therapy allowing to verify dose deposition in a medium externally, potentially in real time, and with no extra dose using scattered x-ray registration. First, using the gDPM simulation package, we obtained the position, momentum direction and energy of the photons scattered outside of a phantom after a MV x-ray beam passed through it. Then, using MATLAB, we collimated the scattered photons and registered them on a photon counting detector. Finally, we related the recorded detector signal to the delivered radiation dose and analyzed the method feasibility. The procedures were carried out on both homogeneous and heterogeneous phantoms.

Introduction

Radiation therapy (RT) is a type of cancer treatment where a high radiation dose is delivered to the tumor while minimizing the exposure of the surrounding healthy tissue. The procedures ensuring the precise and safe delivery of radiotherapeutic dose are called Quality Assurance (QA)[1,2] and govern treatment planning (e.g., contour delineation, dose calculation), treatment delivery (e.g., equipment calibration, patient positioning), and treatment delivery verification (e.g., simulation, physical measurements with radiochromic films). Our project is related to the treatment delivery verification aspect of QA. During RT sessions, the greatest challenges in delivering the prescribed dose precisely come with patient mispositioning, organ movements, and anatomical morphological changes (e.g., tumor shrinkage/growth, tissue inflammation, filling of cavities with mucus)[3], all of which may result in tumor underdose and/or normal tissue overdose. The current solutions include image-guided radiation therapy (IGRT) and adaptive radiotherapy (ART)[3] where physicians use imaging to detect deviations from the initial planning and make the corresponding adjustments. The disadvantage of these techniques is an extra low radiation dose to the patient which, when accumulated over time, may result in developing secondary malignancies[4]. In this project, we implemented a quality assurance method for radiation therapy allowing the verification of dose deposition in a medium externally, potentially in real time, and with no additional dose using scattered x-ray registration.

Materials and Methods

The design of our system is depicted in Figure 1. The system comprises two parts: 1) The simulation of a MV x-ray beam transport through a phantom and the registration of the photons in a scoring volume; 2) The scattered photons' transfer from the scoring volume to a photon counting detector and the relation of the detector signal to the delivered radiation dose.

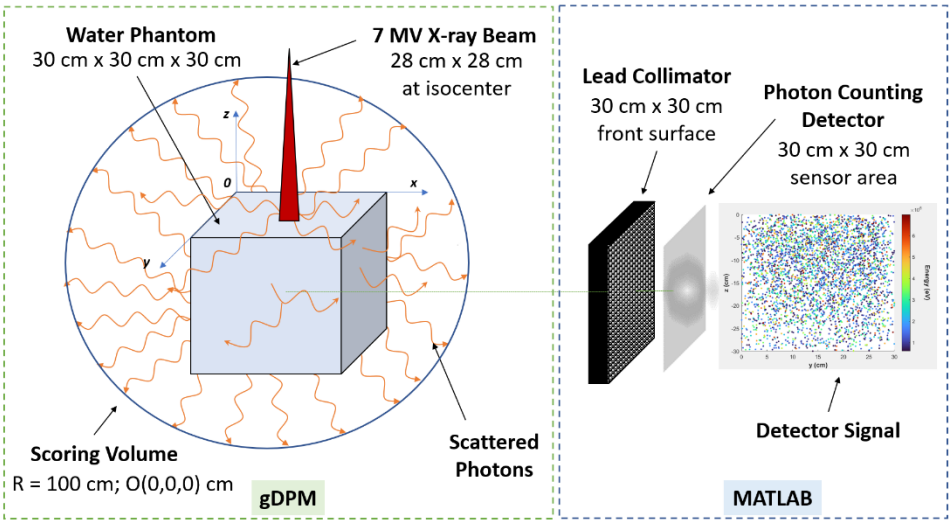

Fig. 1. System design

The first part was done using the gDPM Monte Carlo simulation package[5,6] where the default simulation settings defined a 7 MV X-ray beam hitting, from a distance of 100 cm, the top of a cube-shaped water phantom with a side length of 30 cm; the beam cross-section at the isocenter located inside the phantom at (0, 0, -5) cm was 28 cm x 28 cm; the scoring volume was represented as a sphere surrounding the phantom with the center located at the furthers top left phantom corner and a radius of 100 cm. As photons passed through the phantom, the simulation recorded their energy, momentum direction and position inside the scoring volume (x, y, z- coordinates and radius). If a photon gave up all its energy while interacting with the matter and thus, in theory, got "disappeared" inside the phantom, then its registered position, momentum direction and energy were the ones the photon had right before its death.

The explored simulation input parameters included: the scoring sphere center coordinates and its radius, the phantom density and its dimensions, the beam cross-section dimensions at isocenter, and the number of simulated photons (histories) in the beam. First, as the project idea was to infer on the radiation dose deposition inside a phantom using the information about the photons

scattered outside of the phantom, it was necessary to exclude the photons which did not survive the interactions with the matter. For that purpose, the center of the scoring sphere was aligned with the phantom center, thus allowing to identify the "disappeared" photons by comparing their position radius with the radius of the phantom circumscribed sphere. The scoring sphere radius was kept at 100 cm. Next, we considered the following phantom and beam geometries:

1) Two cube-shaped water phantoms: one with a side length of 30 cm and the beam cross-section of 28 cm x 28 cm at isocenter (defined in the gDPM as default), another one with a side length of 15 cm and the beam cross-section of 7 cm x 7 cm at isocenter.
2) Two cube-shaped heterogeneous phantoms with a side length of 30 cm and the beam cross-section of 28 cm x 28 cm at isocenter: one phantom consisted of water and bone (Figure 2, left) and another one consisted of water, bone, and air (Figure 2, right).

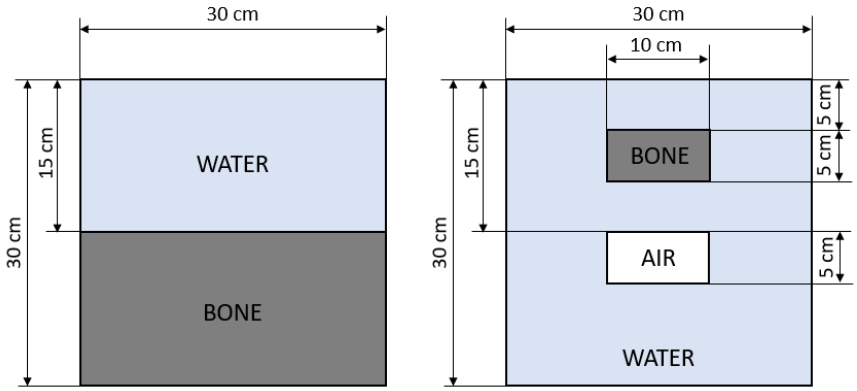

Fig. 2. Heterogeneous phantoms

The heterogeneous phantoms were used to mimic real human body density. Thus, for example, the phantom on the right of Figure 2 represented a case of a morphological alteration where a space between the bone and the air cavity was filled with mucus (water). The phantom design was borrowed from a similar study carried out by other researchers[3]. Both heterogeneous phantoms and the small water phantom were constructed for the simulation by us.

Finally, the gDPM simulated package was run in a GPU-based Google Colab[7] environment. The free of charge platform resources imposed a limit on compute units and memory usage thus allowing us to carry out simulations with at most 10^8 histories which was insufficient for obtaining many scattered photons. To overcome the obstacle, we forced the simulation to record the information on only those photons that would scatter towards the detector sensor based on the x-

coordinate of their momentum direction. The modification reduced the space usage from 1.52 GB to 54.9 MB allowing us to run simulations with 10^{10} histories.

The gDPM output files contained the dose deposited in each phantom voxel, the photon position in the scoring volume as well as their momentum direction and energy. Those gDPM outputs served as inputs to the second system part implemented in MATLAB. Here, we imported the gDPM scoring sphere having the center aligned with the phantom center, and defined a squared detector sensor area such that it would be parallel to the phantom and its size and the vertex coordinates would match the corresponding parameters of the facing phantom side. Next, for one of our photon collimation strategies discussed below, we constructed a 3D lead multi-hole collimator with hexagonal-shape holes. The collimator was positioned in front of the detector and the dimensions of its front face matched the dimensions of the detector sensor. Per the mentor's guidance, we set the collimator thickness to 3.5 cm, the distance between two opposite hole-faces to 1.5 mm, and the distance between two adjacent holes to 0.2 mm.

When transferring scattered photons from the scoring volume to the detector, we first selected the photons that exited the phantom after interacting with the matter. Then, using a parametric representation of photon traveling trajectories, we identified the photons that would collide with the sensor. As those photons were coming from diverse phantom's depths, they would not provide an organized representation of the depth-dose deposition. Therefore, the decision was made to collimate the photons so that only the ones colliding with the detector sensor at an approximately right angle would be considered. For that purpose, we implemented two collimation strategies. The first one was angular filtering where only the photons with a collision angle of 88.5 - 90° were recorded on the detector sensor. The second one was filtering photons using the 3D collimator. Here, to simplify the true physics processes, we recorded on the detector sensor only those photons that passed through the collimator holes without touching the collimator material. The assumption was made based on the fact that the intensity of photons with the energy of 1 MeV (higher than the energies considered in the project) would get reduced by 55% after traveling a distance of 1 cm in lead[8]. Considering the collimator thickness of 3.5 cm, almost none of those photons would reach the detector after moving through the matter if their scattering was ignored.

Once the scattered photons passed one of the collimation procedures, they were then subjected to an energy filtering. In this project, we explored the effect of six energy thresholds: 100 − 1000 keV, 0 − 500 keV, 100 − 500 keV, 100 − 450 keV, 150 − 450 keV, and 200 − 450 keV.

The energy windows were chosen empirically with the first one being arbitrary. Finally, we considered four distances between the phantom and the detector sensor: 5 cm, 15 cm, 30 cm, and 45 cm. The first distance was chosen to place the detector as close to the phantom as possible (while leaving some room for the collimator) to collect more scattered photons. The rationale behind the largest distance was to further filter scattered photons by registering only those that collided with the detector at an angle almost equal to 90°.

The outputs of the system included the visualization of the simulated dose deposition inside the phantom, photon counting detector signal, longitudinal profiles of the simulated dose and scattered photon counts, and the assessment of the correlation between the dose and photon counts' values. The system performance was evaluated using a coefficient of determination (R^2) quantifying the strength of a linear relationship between the longitudinal simulated dose values and the detected scattered photon counts. The desired R^2 was defined to be at least 0.9. The project Wiki-page[9] has documentation providing the detailed description of the system design, requirements and functional specifications, collimator body building, the diagram of the MATLAB computer program structure and its testing, as well as the link to the MATLAB program and commands for running the gDPM in Google Colab.

Results

Figure 3 depicts the gDPM scoring sphere. The accumulation inside the sphere represents the photons "died" in the phantom due to a lack of energy. Their presence indicates the location of the sphere center relative to the phantom. Thus, the left figure shows the scoring sphere with the center at the furthers top left phantom corner which corresponds to the default setup in the gDPM. The right figure shows the sphere with the center aligned with the phantom center, - the setup we adopted for all experiments presented in the report.

Table 1 displays the R^2 values obtained for the cube-shaped water phantom with a side length of 30 cm using angular filtering with different photon energy windows and distances between the phantom and the detector. Figure 4 shows the results obtained for the same phantom using the 3D collimator with the photon energy threshold $200 - 450$ keV and 45 cm phantom-detector distance. Figure 5 shows the results obtained for the water phantom with a side length of 15 cm using angular filtering with the same photon energy threshold and the phantom-detector distance: 2D simulated depth dose profile (top left), heatmap of photon counts on the detector sensor (top, right), longitudinal profiles of the simulated dose and photon counts (bottom left), and simulated dose

values vs. photon counts (bottom right). Figures 6 – 7 present the results for the heterogeneous phantoms obtained under the same collimation conditions.

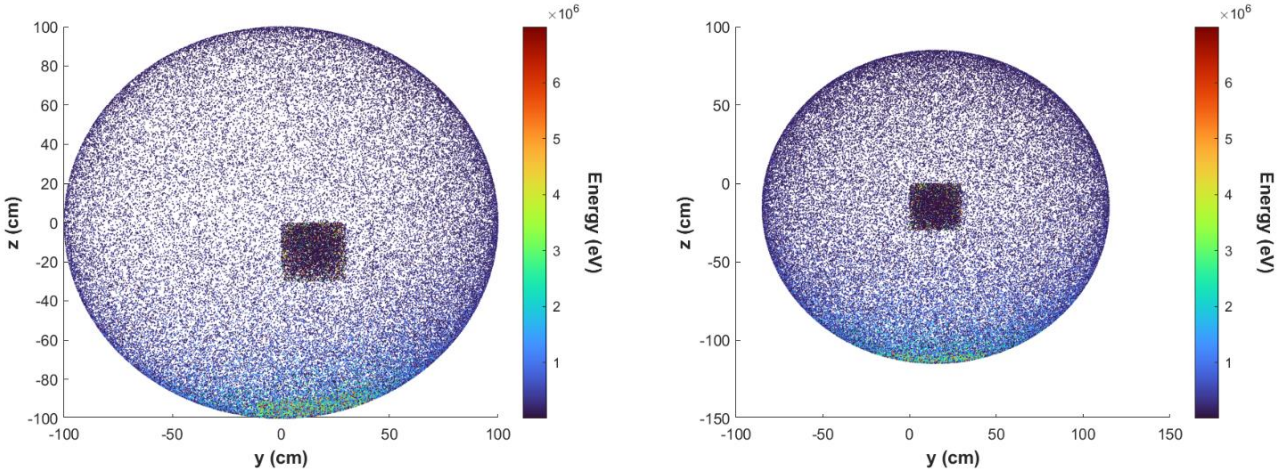

Fig. 3. Scoring sphere center setup

Table 1. R^2 values for the water phantom with a side length of 30 cm using angular filtering

Photon energy, eV	**Distance between the phantom and detector, cm**			
	5	*15*	*30*	*45*
$100 \le E \le 1000$	0.9385	0.9521	0.9593	0.9543
$0 \le E \le 500$	0.8949	0.9043	0.9056	0.8958
$100 \le E \le 500$	0.943	0.9578	0.9679	0.9652
$100 \le E \le 450$	0.9434	0.9585	0.9691	0.9672
$150 \le E \le 450$	0.9468	0.963	0.9767	0.9772
$200 \le E \le 450$	0.943	0.9625	0.9781	**0.98**

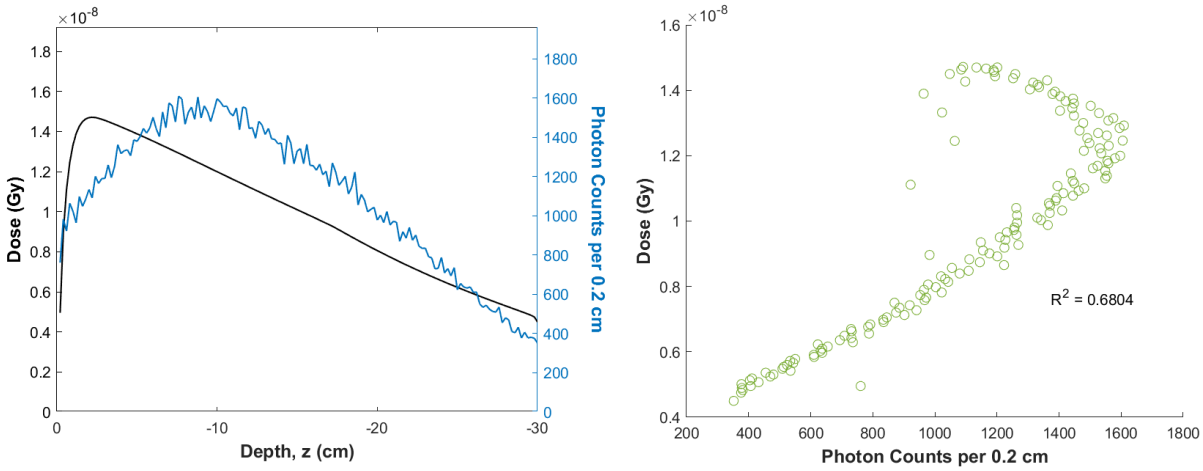

Fig. 4. Results for the water phantom with a side length of 30 cm using 3D collimator with photon energy threshold 200 − 450 keV and 45 cm phantom-detector distance

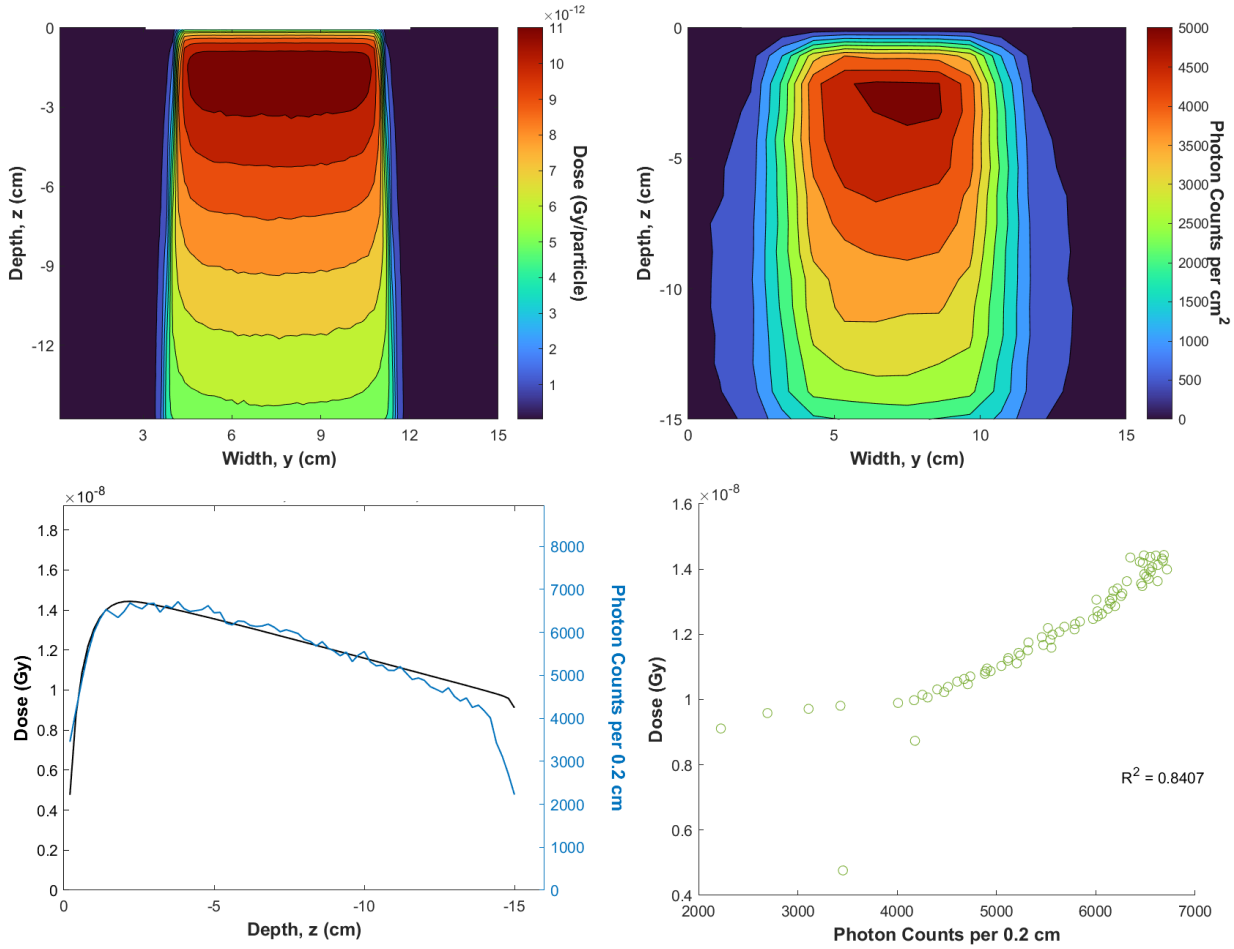

Fig. 5. Results for the water phantom with a side length of 15 cm using angular filtering with photon energy threshold 200 − 450 keV and 45 cm phantom-detector distance

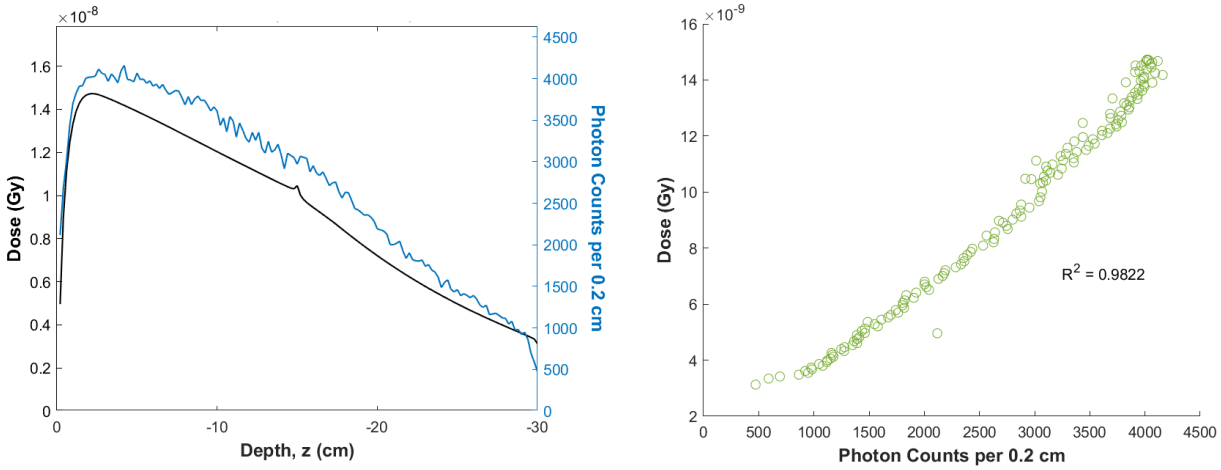

Fig. 6. Results for the water-bone phantom with a side length of 30 cm using angular filtering with photon energy threshold 200 − 450 keV and 45 cm phantom-detector distance

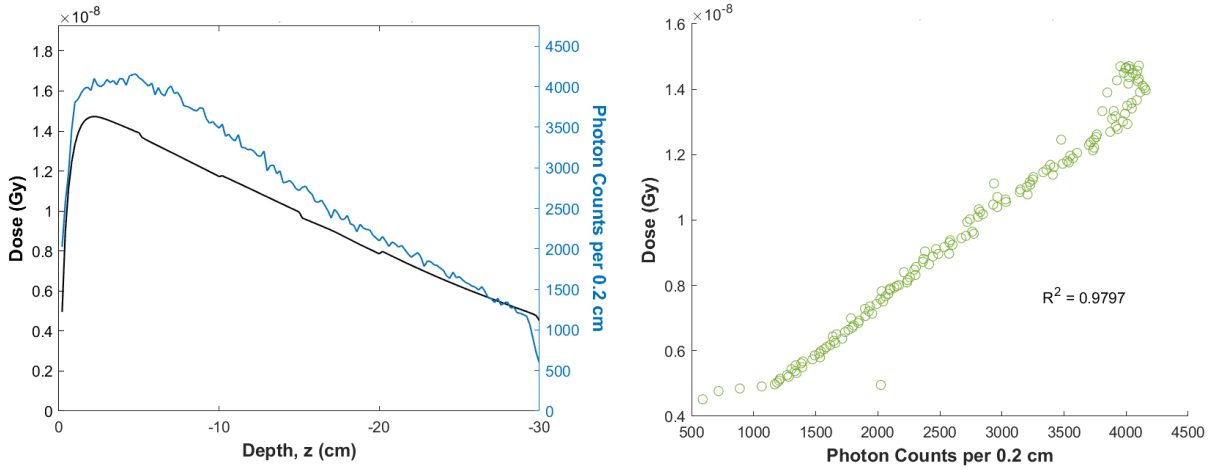

Fig. 7. Results for the water-bone-air phantom with a side length of 30 cm using angular filtering, photon energy threshold 200 − 450 keV, and 45 cm phantom-detector distance

Discussion

The results show a strong correlation between the simulated dose values and the counts of scattered photons. In the case of the cube-shaped water phantom with a side length of 30 cm, the strength of a linear relationship between the dose values and photon counts was found to be the strongest (R^2 = 0.98) when using angular filtering with 200 − 450 keV photon energy threshold and 45 cm phantom-detector distance (Table 1). This can be partly explained by the fact that while a small distance (e.g., 5 cm) allows to collect more photons exiting the phantom, it let many of them to come from slightly different phantom's depths corresponding to 88.5-90° angles which introduces noise to the resulting photon counts profile. A large distance (e.g., 45 cm), on the other hand, filters out scattered photons further by keeping only those that collide with the detector sensor at almost the right angle which, in turn, however, comes at the expense of having a smaller number of photons on the detector sensor. In the case of the water phantom with a side length of 15 cm, under the same collimation conditions (Figure 5), the correlation between the dose and photon counts dropped as compared to the large water phantom because there were twice as few values to compare: the dose and photon counts were collected every 0.2 cm in both large and small phantoms. The longitudinal dose profiles obtained for the water-bone (Figure 6) and water-bone-air (Figure 7) phantoms have clear peaks and valleys corresponding to the changes in the phantoms' density. Such responses are not obvious in the profiles of the scattered photons because the profiles themselves are not smooth as compared to the dose due to the small number of scattered photons considered. This limitation can be addressed by running the simulation with

much larger histories. The high R^2 values (0.9822 for the water-bone phantom and 0.9797 for the water-bone-air phantom) indicate that the scattered photons do correlate with the dose well despite the changes in the phantoms' density.

In the real world, the angular management of radiation is accomplished using collimators. Therefore, in the project, we attempted to build such a device too. While our 3D collimator filters the approaching scattered photons based on the hexagonal-shape holes' geometry, it does not account for all physics processes involved. Thus, for example, it does not consider interactions of the photons with the collimator material which would result in additional scattering causing changes in photon momentum direction and energy. In addition, the chosen collimator geometry might not work well for different photon energy windows. Thus, for example, Figure 4 indicates a significant deviation between the profiles of the dose and the counts of scattered photons with $200 - 450$ keV energy. Finally, the way we built the collimator in MATLAB is not computationally efficient: a single run of the code takes more than three hours, while angular filtering takes a few minutes to complete given that the gDPM output files are read. That is why we used the collimator in the project only once.

In a similar study[3] carried out by other researchers, the whole system (including the 3D collimator and the detector sensor) was built in Geant4[10],- another Monte Carlo simulation toolkit for modeling radiation passage through a matter. Such a technical approach is supposed to provide more realistic results because the interactions of the scattered radiation with all system objects are considered. The authors reported the highest $R^2 = 0.94$ observed for scattered photons with the nominal energy of 600 keV.

Conclusions and Future Work

The results of the current project and the similar study[3] show the presence of a strong correlation between the radiation dose deposited in a phantom and the counts of scattered photons which indicates the method's potential to be used in clinic for dosimetric verification and treatment monitoring. As Dr. Jia and Dr. Su noted, the next step would be to characterize the linear relationship between these data while determining possible confounding variables. Other photon energy thresholds, distances between the phantom and the detector, as well as the collimator geometry could be also explored. The longitudinal dose values could be subjected to weighting to distinguish the amount of dose deposited near the phantom side where the scattered photons are collected. Finally, the whole QA system could be implemented in the gDPM or another simulation

package to account for the interactions of scattered photons with all system units. Once the simulation studies are completed, it would be important to compare the results with physical measurements to validate the technique.

Management

Activity	Done by
Class Assignments: • Project proposal presentation slides • Project proposal written report • Background reading presentation slides • Background reading written report • Checkpoint presentation slides • Poster teaser presentation slides • Project Wiki-page • Documentation (code, system design and requirements, system testing) • Final project report • Final project poster	90% Tatiana 10% Samuel
Main Code Parts*: • gDPM compilation on Google Colab	Samuel
• gDPM scoring sphere and MATLAB system setup	Tatiana
• Photon transfer from the scoring sphere to the detector using parametric representation of photon trajectories	Tatiana
• Photon collimation using angular filtering	Tatiana
• 3D collimator body	Samuel
• Photon collimation by the 3D collimator	30% Tatiana 70% Samuel
• Definition files for 2 heterogeneous phantoms	Samuel
• Studies of the water phantom size, photon energy thresholds, and phantom-detector distances	Tatiana
• Statistical analysis	Tatiana
• The reduction of the gDPM output files' size to enable simulations with more histories	Samuel
• Unit-testing of the code functions	Samuel
*Each code function has a header comment describing the function purpose, inputs, outputs, and the author.	

References

1. World Health Organization. (1988). Quality Assurance in Radiotherapy: a Guide Prepared Following a Workshop Held at Schloss Reisensburg, Federal Republic of Germany, 3-7 December1984. Geneva
2. Glide-Hurst, C.K., & Chetty, I.J. (2014). Improving radiotherapy planning, delivery accuracy, and normal tissue sparing using cutting edge technologies. *Journal of Thoracic Disease*, *6* (4), p.303–318
3. Cunha, M., et al. (2013). Dose-free monitoring of radiotherapy treatments with scattered photons: Concept and simulation study. *IEEE Transactions on Nuclear Science, 60* (4), p. 3119-3126
4. Dzierma, Y., Mikulla, K., Richter, P. Bell, K., Melchior, P., Nuesken, F., & Rübe, C. (2018). Imaging dose and secondary cancer risk in image-guided radiotherapy of pediatric patients. *Radiation Oncology, 13,* 168.
5. Jia, X. & Jiang, S.B. (2011). gDPM v2.0. A GPU-based Monte Carlo simulation package for radiotherapy dose calculation. The Center for Advanced Radiotherapy Technologies (CART), UCSD.
6. Jia, X., Ziegenhein, P., & Jiang, S. B. (2014). GPU-based high-performance computing for radiation therapy. *Physics in Medicine and Biology, 59*(4), p. R151–R182.
7. Google Colab. Retirved from https://colab.research.google.com/
8. Johns, H.E. & Cunningham, J.R. (1983). The Physics of Radiology, 4th Edition, Table A-4i. Radiological Properties of Lead, p. 736
9. CIS Spring 2023 Projects (2023). 03: Quality assurance of radiotherapy treatment using scattered x-ray. Retrieved from https://ciis.lcsr.jhu.edu/doku.php?id=courses:456:2023:projects
10. Geant4. Retrieved from https://www.geant4.org/